Acta Biomaterialia 8 (2012) 333–340

Contents lists available at SciVerse ScienceDirect

Acta Biomaterialia

journal homepage: www.elsevier.com/locate/actabiomat

Structural characterization and physical properties of P_2O_5–CaO–Na_2O–TiO_2 glasses by Fourier transform infrared, Raman and solid-state magic angle spinning nuclear magnetic resonance spectroscopies

Azadeh Kiani [a], John V. Hanna [b], Scott P. King [b], Gregory J. Rees [b], Mark E. Smith [b], Nima Roohpour [c], Vehid Salih [a], Jonathan C. Knowles [a,d,*]

[a] Division of Biomaterials and Tissue Engineering, University College London Eastman Dental Institute, 256 Gray's Inn Rd., London WC1X 8LD, UK
[b] Department of Physics, University of Warwick, Coventry CV4 7AL, UK
[c] School of Engineering and Materials Science, Queen Mary University of London, London E1 4NS, UK
[d] WCU Research Centre of Nanobiomedical Science, Dankook University, San#29, Anseo-dong, Dongnam-gu, Cheonan-si, Chungnam 330-714, South Korea

ARTICLE INFO

Article history:
Received 21 June 2011
Received in revised form 22 August 2011
Accepted 26 August 2011
Available online 31 August 2011

Keywords:
Phosphate glass
^{31}P NMR
Degradation
Ion release
Phosphate species

ABSTRACT

Phosphate-based glasses have been investigated for tissue engineering applications. This study details the properties and structural characterization of titanium ultra-phosphate glasses in the $55(P_2O_5)$–$30(CaO)$–$(25-x)(Na_2O)$–$x(TiO_2)$ $(0 \leqslant x \leqslant 5)$ system, which have been prepared via melt-quenching techniques. Structural characterization was achieved by a combination of X-ray diffraction (XRD), and solid-state nuclear magnetic resonance, Raman and Fourier transform infrared spectroscopies. Physical properties were also investigated using density, degradation and ion release studies; additionally, differential thermal analysis was used for thermal analysis of these glasses. The results show that with the addition of TiO_2 the density and glass transition temperature increased whereas the degradation and ion release properties are decreased. From XRD data, TiP_2O_7 and CaP_2O_6 were detected in 3 and 5 mol.% TiO_2-containing glasses. Magic angle spinning nuclear magnetic resonance results confirmed that as TiO_2 is incorporated into the glass; the amount of Q^3 increases as the amount of Q^2 consequently decreases, indicating increasing polymerization of the phosphate network. Spectroscopy results also showed that the local structure of glasses changes with increasing TiO_2 content. As TiO_2 is incorporated into the glass, the phosphate connectivity increases, indicating that the addition of TiO_2 content correlates unequivocally with an increase in glass stability.

1. Introduction

Biodegradable materials with their great potential in tissue engineering applications have been the subject of much interest in recent studies. Numerous bioactive glasses have been developed for repair and reconstruction of bony tissue. The similarity of phosphate-based glasses to that of mineral phase of the hard tissue, plus their biodegradability and bioactivity, make these glasses of major interest as scaffolds for tissue engineering [1–3]. Phosphate glasses offer the property of being completely degradable in aqueous media; more interestingly, this solubility can be controlled via altering the glass chemistry to suit the end application.

Ternary phosphate glass (P_2O_5–CaO–Na_2O) has poor chemical durability, being too soluble for applications requiring long-term stability. To circumvent this problem, various modifying metal oxides have been incorporated into the glass system to control the degradability that can be adjusted to the end application. Several metal oxides such as MgO, CuO, ZnO, Fe_2O_3 and Al_2O_3 [4–8] have been tried previously to control the degradability of meta- and poly-phosphate glasses, and TiO_2 has been shown to be efficient for improving chemical durability and mechanical properties of these glasses [9–11]. TiO_2 was found to induce calcium phosphate surface nucleation in CaO–P_2O_5-based systems [12]. TiO_2 has also been found to stabilize the phosphate glass network by forming Ti–O–P rather than P–O–P bonds [13]. Furthermore, in glasses at the metaphosphate composition with additions of between 0 and 5 mol.%, increased gene expression in vitro and increased bone formation in vivo may be seen at the highest TiO_2 content. The exact reason for this is ambiguous, but may be either a minimization of pH changes or that the Ti^{4+} ions being released actually play a biological role.

So far, the structure of meta-phosphate glasses has been extensively studied, alongside poly-phosphate glasses mainly containing

* Corresponding author at: Division of Biomaterials and Tissue Engineering, University College London Eastman Dental Institute, 256 Gray's Inn Rd., London WC1X 8LD, UK. Tel.: +44 2034 561189.
E-mail address: j.knowles@ucl.ac.uk (J.C. Knowles).

1742-7061/$ - see front matter © 2011 Acta Materialia Inc. Published by Elsevier Ltd. All rights reserved.
doi:10.1016/j.actbio.2011.08.025

45 mol.% P_2O_5. However, there is still little known about the structure of ultra-phosphate glasses, in particular the impact of incorporation of metal oxides on their structure and properties. Thus, in the current work the effect of TiO_2 incorporation on high P_2O_5-containing glasses (55 mol.% P_2O_5) in the ultra-phosphate region has been investigated. The structure of this series of glasses is analyzed by powder X-ray diffraction (XRD), and Fourier transform infrared, Raman and solid-state magic angle spinning nuclear magnetic resonance (MAS-NMR) spectroscopies. The MAS-NMR in particular gives us much structural information about Q speciation, whereby Q^0 represents isolated PO_4^{3-} units with four non-bridging oxygens (NBO), Q^1 represents a phosphorous with one bridging oxygen (BO) and three NBO, Q^2 represents a phosphorous with two BOs and two NBOs and Q^3 is a phosphorous with three BOs and one NBO. In addition, thermal and physical properties of these glasses are investigated using differential thermal analysis (DTA) and degradation (and ion release) studies.

2. Methods and materials

2.1. Manufacture of the glasses

NaH_2PO_4, $CaCO_3$, P_2O_5 and TiO_2 (BDH, Poole, 98%, UK) have been used as precursor materials. Glass rods of 15 mm diameter, with different TiO_2 content (0, 1, 3 and 5 mol.%, designated Ti0%, Ti1%, Ti3% and Ti5%), were prepared via a melt-quenching route at the corresponding temperatures and hold times given in Table 1. The actual procedure of making the glass via this melt-quench process and preparing the disks have been described previously in detail [11].

2.2. Bulk glass characterization

2.2.1. Density measurements

Density measurements were carried out in triplicate using Archimedes' principle, on an analytical balance (±0.1 mg, Mettler Toledo, UK) with an attached density kit and ethanol was used as immersion liquid.

2.2.2. Thermal analysis

Thermal characterization was carried out using a Setaram differential thermal analyzer (Setaram, France) on powdered glass samples to determine glass transition (T_g), crystallization (T_c), and (T_m) melting temperatures at a heating rate of 20 °C min^{-1} up to 1000 °C.

2.2.3. Degradation study

The degradation studies were carried out on triplicates using a weight loss method in deionized water at 37 ± 1 °C. The surface area of the glass disks was calculated from dimensions obtained via a pair of Mitutoyo Digimatic vernier calipers. Glass disks then were placed in containers holding 25 ml of high purity water (18.2 MΩ cm^{-1} resistivity) prepared from a PURELAB UHQ-PS (Elga Labwater, UK) with a pH of 7 ± 0.1. At various time points up to 336 h, the solution was removed for ion release study; then the disks were taken out, dried with tissue and weighed, and then placed in a fresh solution of deionized water and replaced in an incubator at 37 ± 1 °C. The data were plotted as cumulative degradation, percentage weight loss per unit area as a function of time.

Table 1
The glass compositions and melting/annealing temperatures used.

Glass composition (mol.%)			Processing temperature (°C)/time (h)		
P_2O_5	CaO	Na_2O	TiO_2	Melt	Annealing
55	30	15	0	1100/1	350/1
55	30	14	1	1300/3	350/1
55	30	12	3	1300/3	370/1
55	30	10	5	1300/3	400/1

2.2.4. Ion release analysis

The degradation medium was analyzed simultaneously for cation (Na^+ and Ca^{2+}) and anion (PO_4^{3-}, $P_2O_7^{4-}$, $P_3O_9^{3-}$, and $P_3O_{10}^{5-}$) release, using ion chromatography (Dionex, UK). Inductively coupled plasma mass spectroscopy (ICP-MS) was used to measure the amount of Ti^{4+} release, as described previously [11].

2.3. Structural characterization

2.3.1. X-ray powder diffraction analysis (XRD)

XRD was performed to check that the glasses were amorphous and to identify any crystalline phases present, following annealing of the glass at the temperatures obtained from DTA. Samples were annealed at T_c + 5 °C. The data were collected on a Bruker D8 Advance Diffractometer (Bruker, UK) in flat plate geometry, using Ni-filtered Cu Kα radiation and a Bruker Lynx Eye detector. Data were collected from 2θ = 10–100° with a step size of 0.02° and a count time of 12 s per point. The phases were identified using the Crystallographica Search-Match (CSM) software and the International Center for Diffraction Data (ICDD) database (vols. 1–42) [14].

2.3.2. Raman spectroscopy

Raman spectra of the glass disks were obtained using a Nicolet Amelga XR dispersive Raman spectrophotometer (Thermo Scientific, USA), equipped with a non-polarized 785 nm laser. The spectra were obtained in the range 4000–400 cm^{-1} over an average of 128 scans and 1.0 s exposure time in Micro Raman compartment with 10× objective.

2.3.3. Fourier transform infrared spectroscopy

FTIR spectra of the glasses were obtained using a Nicolet 8600 FTIR spectrometer (Thermo Scientific, USA) in conjunction with a MTEC Photoacoustic Spectrum (PAS) detector. Spectra were obtained in the mid-infrared region (4000–400 cm^{-1}) at 4 cm^{-1} resolution and averaging 256 scans.

2.3.4. Solid state NMR

Solid-state ^{31}P MAS NMR spectra were acquired at a Larmor frequency of 161.923 MHz on a Bruker DSX-400 spectrometer (9.4 T), using a 3.2 mm double resonance probe spinning at 12 kHz. All ^{31}P data were acquired using a one-pulse experiment with proton decoupling during acquisition, employing a $\pi/2$ pulse length of 4 μs. A recycle delay of 30 s was used to ensure that saturation did not occur and that all spectra represented a quantitative description of the phosphorus speciation. Each ^{31}P data set represented 100 co-added transients, and all ^{31}P spectra were referenced to 85% H_3PO_4 via a secondary reference of solid $NH_4H_2PO_4$ (0.9 ppm).

Solid-state ^{23}Na MAS-NMR spectra were acquired at Larmor frequencies of 105.81 and 158.71 MHz on Bruker DSX-400 (9.4 T) and Bruker Avance II-600 (14.1 T) spectrometers, respectively. A 3.2 mm Bruker double resonance probe was used at both fields with a spinning frequency of 20 kHz. At each field ^{23}Na data were acquired using a one-pulse experiment; a "non-selective" (solution) $\pi/2$ pulse time of ~6 μs was calibrated on solid NaCl from which a "selective" (solid) θ pulse times of ~1 μs were employed to ensure quantitative estimates and to avoid line shape distortions [15]. A recycle delay of 5 s was implemented, and 1400 and 500 transients were acquired at 9.4 and 14.1 T, respectively. All ^{23}Na

spectra were referenced to 1 M NaCl (aq.) (δ 0.0 ppm) via the secondary reference of solid NaCl (δ 7.2 ppm).

All experimental ^{31}P MAS-NMR data were simulated and deconvoluted using the DMFit software package [16], while the corresponding ^{23}Na MAS NMR data were simulated using both the DMFit and Quadfit [17] software packages.

3. Results and discussion

3.1. Density

Fig. 1 shows the density (g cm^{-3}) as a function of TiO_2 content. It can be clearly seen that the density of the bulk glass increases from 2.56 g cm^{-3} in the Ti0% glass to 2.58 g cm^{-3} in the Ti5%$_2$ glass. This might be as a result of formation of a denser glass structure associated with close packing of atoms by the strong P–O–Ti bonds [18].

3.2. Thermal analysis

Fig. 2 shows the DTA trace of these glasses. The clear feature is attributed to the glass transition temperature (T_g), which increases from 381 °C in Ti-free glass to 437 °C the glass containing 5 mol.% TiO_2. The upward peaks are exothermic and represent the glass crystallization temperature (T_c), which also shows an increase with the addition of TiO_2 from 590 to 712 °C. The endothermic peaks (downward), however, define the melting point (T_m), increased by 100 °C by the addition of TiO_2.

3.3. Degradation study

Fig. 3 shows the cumulative degradation presented as percentage weight loss per unit area as a function of time for all tested glass samples. The weight loss per unit area increased over time for all tested glass samples. However, the degradation rate showed a reduction on increasing the TiO_2 content, which could be due to the formation of a more highly cross-linked dense structure formation that resists degradation, which is also consistent with the T_g and density data.

3.4. Ion release

The cumulative cation release, in terms of Na^+ and Ca^{2+}, as a function of time is shown in Fig. 4a and b. As can be observed there is an increase in the release of both ions over the time for all glass

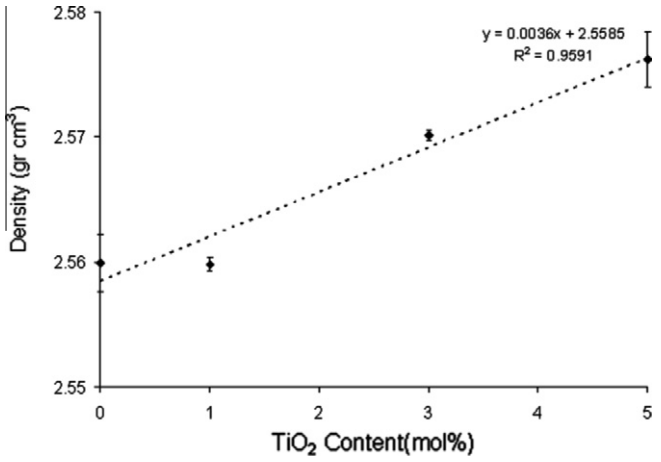

Fig. 1. Density (g cm^{-3}) as a function of TiO_2 content (mol.%), indicating the impact of titanium concentration on the glass density.

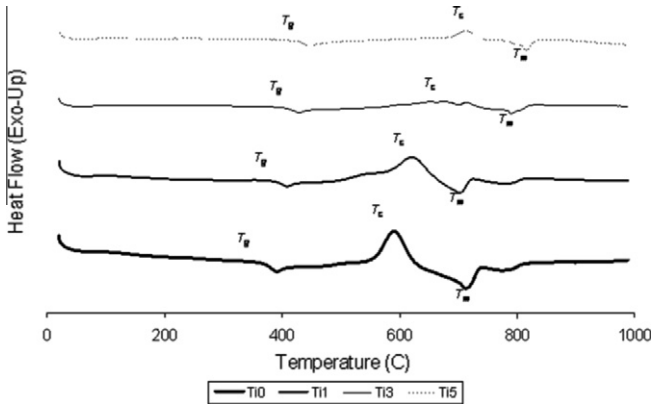

Fig. 2. DTA trace of Ti-free and Ti-containing (1, 3 and 5 mol.%) glasses, when heated up to 1000 °C.

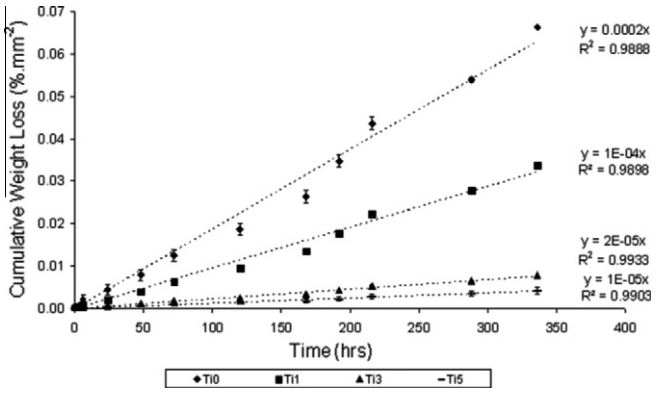

Fig. 3. Degradation presented as cumulative weight loss %/surface area for TiO_2-containing glasses (1, 3 and 5 mol.%) compared to TiO_2-free glass as a function of time.

compositions, and a reduction with incorporation of TiO_2, which reflects the degradation behavior.

The cumulative release patterns for different anions, PO_4^{3-}, $P_3O_9^{3-}$, $P_2O_7^{4-}$, and $P_3O_{10}^{5-}$, follow the same trend as cation release and are shown in Fig. 5a–d).

3.5. X-ray powder diffraction

For the Ti0% glass and the Ti1% glass, a $NaCa(PO_3)_3$ phase (ICCD No. 23–669) was identified from the Crystallographica database. In the Ti3% and Ti5% glasses, CaP_2O_6 (ICDD No. 11–39) as the main crystalline phase and TiP_2O_7 (ICCD No. 38–1468) as a secondary crystalline phase were detected.

3.6. Raman spectroscopy

Raman spectroscopy (Fig. 6) shows that the structure of these phosphate glasses was slightly changed upon addition of titanium. Three intense bands are clearly visible in the Raman spectrum. The band at ~695 cm^{-1} corresponds to the symmetric stretching mode of P–O–P bridging oxygens, $(POP)_{sym}$, between Q^3 phosphate tetrahedra. This peak has shifted from 695 cm^{-1} in the Ti0% glass sample to 705 cm^{-1} in the Ti5% sample, indicating an increase in average length of the P–O–P bond. The peak at ~1180 cm^{-1} is attributed to the symmetric stretching mode of O–P–O non-bridging oxygens, $(PO_2)_{sym}$, in Q^2 phosphate tetrahedra. The band at ~1280 cm^{-1} is attributed to asymmetric stretch of O–P–O, $(PO_2)_{asym}$. The relative intensity of the symmetric stretch of the P=O

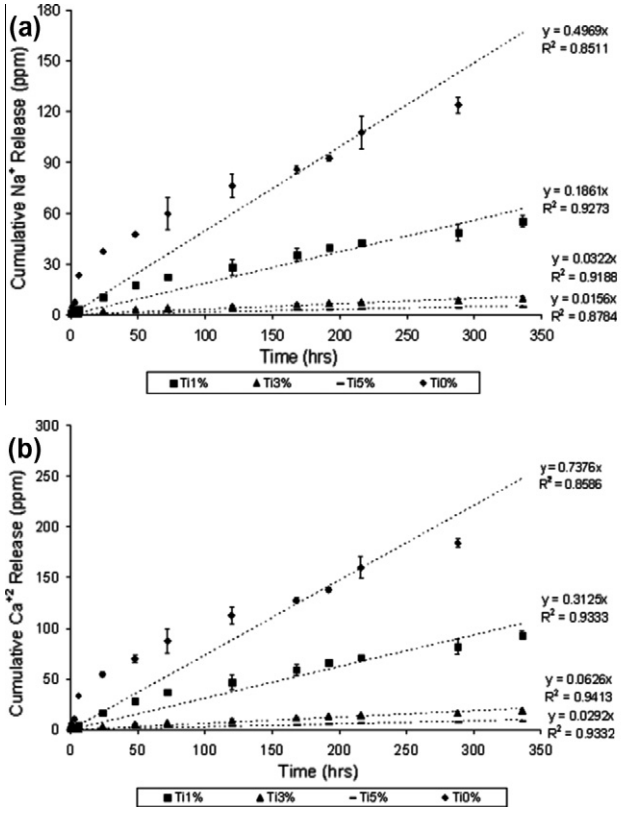

Fig. 4. Cumulative cation release: (a) Na^+ and (b) Ca^{2+}, presented as ppm ion release as a function of time for Ti-free glass compared to Ti-containing (1, 3 and 5 mol.%) glasses.

bond (near 1370 cm^{-1}) has increased by incorporation of TiO_2 up to 5%, indicating a more cross-linked structure; i.e., a greater Q^3 content [19]. Moreover, the peak at ~930 cm^{-1} corresponds to a Ti–O band, the intensity of which increases with increasing Ti content.

3.7. FTIR analysis

FTIR spectra of these glasses are presented in Fig. 7a and b. The broad peak at ~3460 cm^{-1} is due to symmetric stretching of O–H groups (originated from absorbed water). There is a broad peak at ~1666 cm^{-1} assigned to C═O, which is thought to originate from the CO_2 in the atmosphere. The FTIR peaks observed for samples containing TiO_2 are mainly due to the phosphate network which appears in the range 1400–500 cm^{-1}. The band at ~1300–1250 cm^{-1} is assigned to asymmetric stretching modes, υ_{as} (O–P–O), of the two non-bridging oxygen atoms bonded to a phosphorus atom in a Q^2 phosphate tetrahedron. The FTIR band at 1147 cm^{-1} corresponds to symmetric stretch of $(O–P–O)^-$. The absorption bands near 1100 and 1000 cm^{-1} are assigned to the asymmetric and symmetric stretching modes of chain-terminating Q^1 groups (υ_{as} $(PO_3)^{2-}$, υ_s $(PO_3)^{2-}$), respectively [20].

The absorption bands υ_{as}(P–O–P) and υ_s(P–O–P) occurring at ~900 and 750 cm^{-1} are assigned, respectively, to the asymmetric and symmetric stretching of the bridging oxygen atoms bonded to a phosphorus atom in a Q^2 phosphate tetrahedron [21,22].

The intensity of the band near 1070 cm^{-1}, which is attributed to $(PO_4)^{3-}$ end groups (Q^0), tends to decrease with increasing TiO_2 content. It is shown that the absorption bands of the amplitudes of $(PO_4)^{3-}$ groups near 1070 and 960 cm^{-1} decrease with increasing titania content.

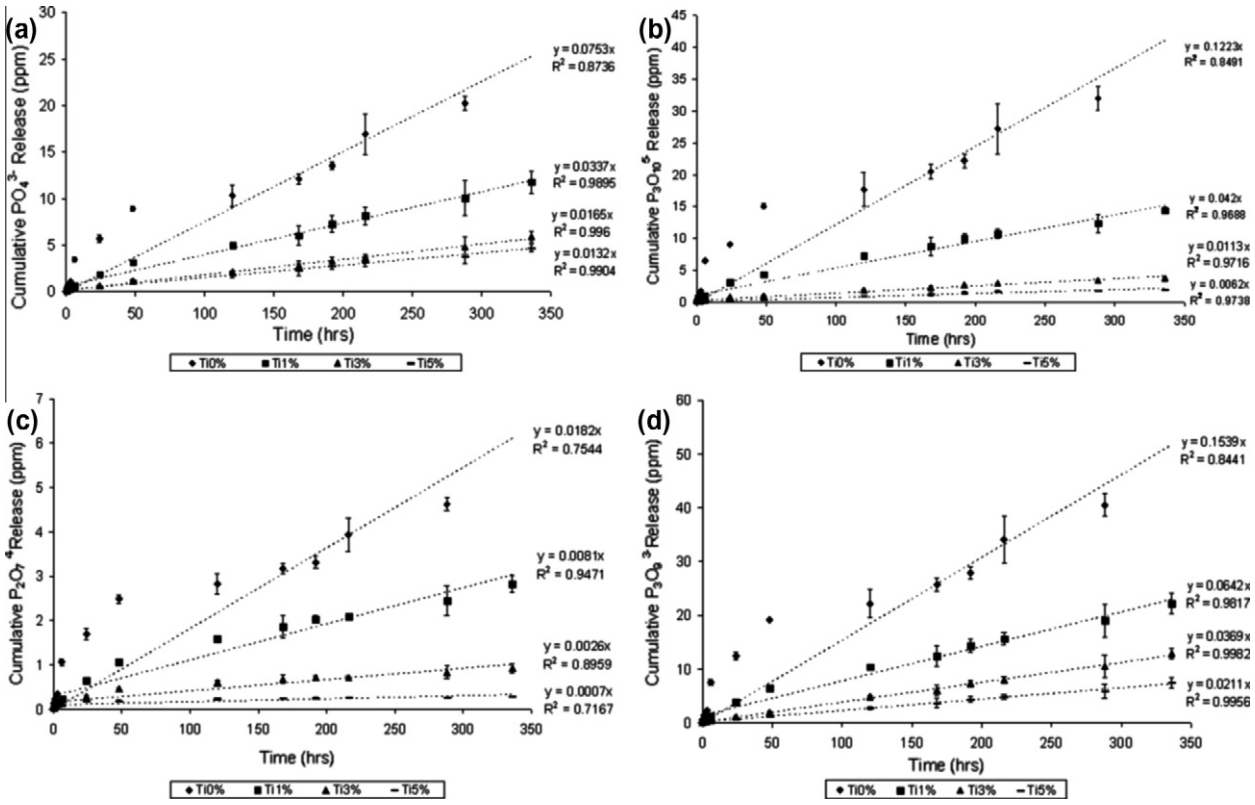

Fig. 5. Cumulative anion release: (a) PO_4^{3-}, (b) $P_3O_{10}^{5-}$, (c) $P_2O_7^{4-}$, and (d) $P_3O_9^{3-}$, presented as ppm ion release as a function of time for Ti-free glass compared to Ti-containing (1, 3 and 5 mol.%) glasses.

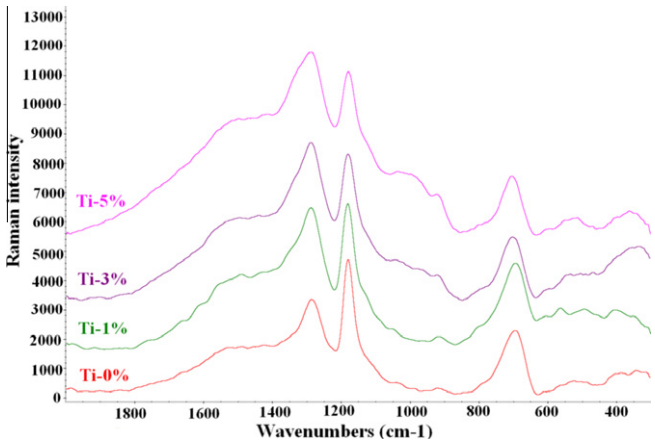

Fig. 6. Raman spectra of TiO_2-free and TiO_2-containing (1, 3 and 5 mol.%) glasses.

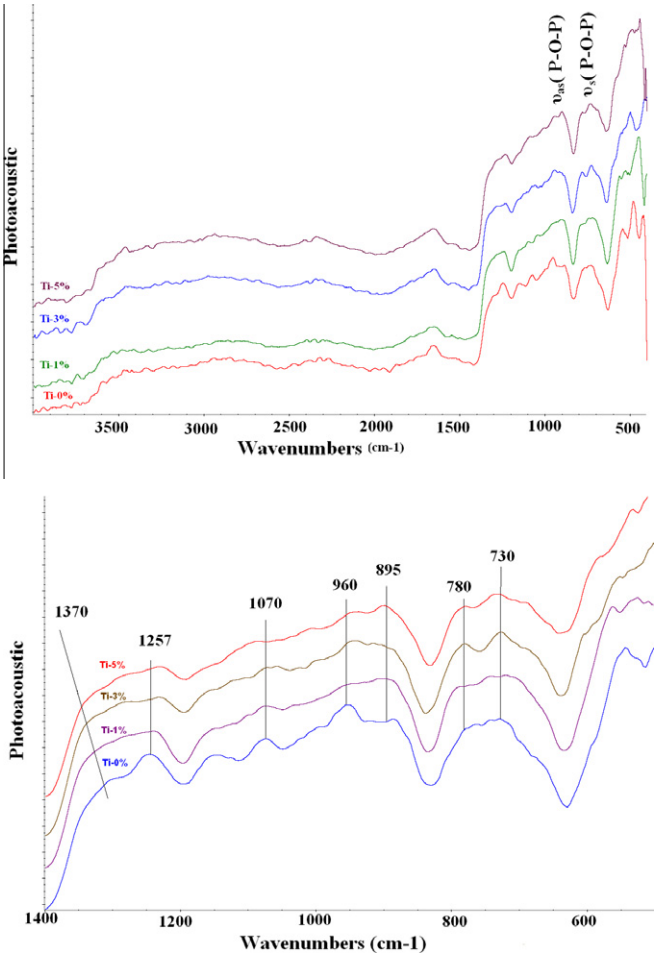

Fig. 7. (a) FTIR spectra of TiO_2-free and TiO_2-containing (1, 3 and 5 mol.%) glasses. (b) An expanded view of the region from 1400 to 500 cm^{-1} for TiO_2-free and TiO_2-containing (1, 3 and 5 mol.%) glasses.

Decreasing Q^1 and Q^0 groups indicates that the relative content of non-bridging oxygen, which may be replaced by the formation of Ti–O–P bonds, decreases on incorporation of TiO_2. In addition, the asymmetric stretching band of P–O–P near 900 cm^{-1} initially shifts to higher frequencies as the amount of the Ti increases.

In an expanded view of the region up to 1400 cm^{-1}, Fig. 7b, an increase in the characteristic of Q^3 υ (P=O) band (1300–1400 cm^{-1}) and decrease in the intensity of Q^2 υ_{as} (PO_2) band at 1257 cm^{-1} are evident [23]. The Q^2 υ_{as} (O–P–O) band (at 1257 cm^{-1}) has also shifted to a lower wave number by the addition of TiO_2. Furthermore, the peak around 1070 and 960 cm^{-1} could be related to vibration of (PO_3^{2-}) [24], which disappeared (reduced intensity) with Ti addition.

3.8. Solid state MAS-NMR

3.8.1. Solid-state ^{31}P MAS-NMR

^{31}P NMR is a valuable tool in characterizing structures of phosphate-type glasses due to the chemical shifts being sensitive to the phosphorus environment present. The phosphate bonding is described via Q^n species, where the superscript n refers to the number of bridging oxygens per tetrahedron. Vitreous P_2O_5 consists only of cross-linked Q^3 tetrahedra; however, with the increase of network modifier cations such as Na^+ and Ca^{2+}, Q^3 is depolymerized to chain-like Q^2 and then further depolymerized to Q^1 and Q^0 units [25].

Fig. 8 shows the ^{31}P MAS-NMR spectra for the glasses with increasing TiO_2 content. The ratio of the two resonances was obtained by fitting the resonances with Gaussian line shapes and summing the intensities of the isotropic peaks and the full span of corresponding spinning sidebands.

Table 2 shows the isotropic shifts along with the relative intensities for the two phosphorus sites, with the Q^n species being assigned using the isotropic shifts given in Brow et al. [25].

Fig. 9a shows how varying TiO_2 results in a change in the abundance of the Q^n species. It can be seen that as the amount of TiO_2 increases the amount of Q^3 increases (from 28% to 40%) as the amount of Q^2 consequently decreases, indicating increasing polymerization of the phosphate network.

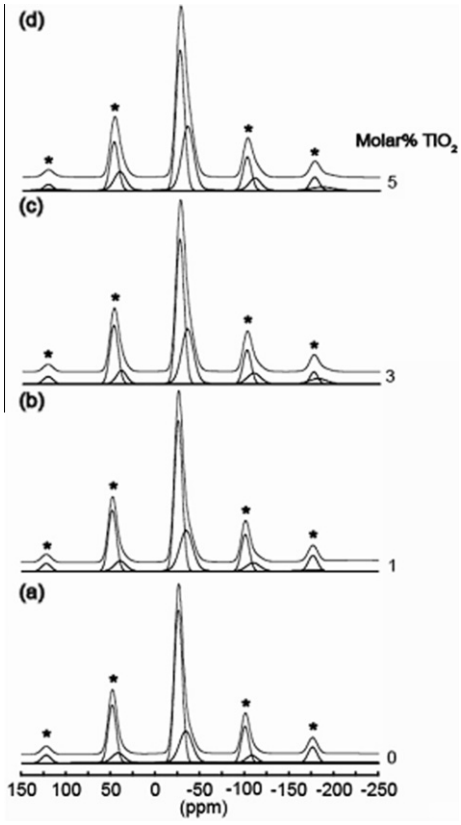

Fig. 8. ^{31}P MAS-NMR spectra obtained for the glass samples with increasing mol.% TiO_2: (a) Ti-free, (b) TiO_2 1 mol.%, (c) TiO_2 3 mol.% and (d) TiO_2 5 mol.%. The asterisks represent the deconvoluted spinning side bands.

Table 2
Summary of the ^{31}P isotropic chemical shifts (δ_{iso}), and relative intensities for the phosphate glasses.

TiO_2 content (%)	Q^2		Q^3	
	δ_{iso} (ppm) ±0.3	% Rel. int. ±1	δ_{iso} (ppm) ±0.3	% Rel. int. ±1
0	−25.7	72	−34.0	28
1	−26.0	68	−34.7	32
3	−26.1	65	−34.4	35
5	−26.1	60	−33.3	40

Quantitatively the average P–O–P coordination (N_{P-O-P}) is defined as:

$$N_{P-O-P} = 2f_{Q^2} + 3f_{Q^3} \quad (1)$$

where f_{Q^n} refers to the fraction of the Q^n group [11].

It is found that the average Q^n increases from 2.28 to 2.40 with the increase in TiO_2 content, with a value of 2 indicating solely Q^2 species and a value of 3 solely Q^3 species present. This increase in connectivity of the network with increasing TiO_2 is consistent with results found previously by our group, where it was found that the substitution of TiO_2 for Na_2O in the initial glass composition resulted in the Ti^{4+} rather than carrying out the role of network modifier (as the Na^+), to cause cross-linking between oxygens [11].

The presence of Q^3 and Q^2 in these glasses is consistent with the work of Brow et al., who found that in glasses with a P_2O_5 content of above 50 mol.% the phosphate species present are Q^3 and Q^2, as found in our 55 mol.% samples [25]. In addition the previous study by our group where glasses of 45 mol.% P_2O_5 were investigated the Q^2 and Q^1 found is also in agreement with previous studies [11,25]. These results show as expected that with an increase of P_2O_7 the connectivity of the glass increases. There is an anomaly between the FTIR data and the ^{31}P NMR data in that the FTIR data show the presence of both Q^1 and Q^0 species, but these were not seen in the NMR data. The presence of these species may be due to sample preparation, but it should be borne in mind that the levels of these species, as seen in the FTIR data, is extremely low and this may be why they are not seen in the NMR, which has a detection limit of ~1 mol.%. Also ^{31}P NMR is directly quantitative whereas careful calibration is needed to quantify the Q^n speciation from the observed FTIR reflections.

^{31}P isotropic chemical shifts should give an indication to the local arrangement of the glass, both the covalent bonding and ionic interactions with Ca^{2+} and Na^+. Fig. 9b shows the change in chemical shift of the ^{31}P resonances as the amount of TiO_2 is increased. It would be expected that as the amount of TiO_2 is increased the chemical shifts should move upfield, as found in our previous studies [11,19,26–27]. This is due to the formation of Ti–O–P bonds, where now the Ti^{4+} can create several cross-links between oxygen sites, unlike the Na^+ ion. As more cross-links are formed in the glass the charge on the oxygen is displaced away from the P–O bonds, leading to the nuclei becoming more shielded, producing a change in chemical shift. However, this is not found in these glasses as there appears to be no obvious trend in the chemical shift with increasing TiO_2. This could be explained due to all the glasses having a very condensed network, as indicated by the high Q^3 values. This would leave little room for the Ti^{4+} to make much difference in the number of cross-links between oxygen sites, and hence this corresponding change in chemical shift would then only be small.

3.8.2. Solid-state ^{23}Na MAS-NMR

NMR is a commonly used, highly sensitive probe of sodium environments in disordered glassy structures, as NMR does not depend on long-range order required in other analytical techniques. It is commonly used in sodium silicate and aluminosilicate glasses to distinguish the coordination environments and the structural connectivity of neighboring network formers and modifiers [28]. Sodium phosphate glasses have a very narrow chemical shift range from −5.4 to −9.3 ppm, with less shielding (more positive ppm) with increasing Na_2O content in the glass [25].

Fig. 10 shows the ^{23}Na MAS-NMR at 14.1 and 9.4 T for the samples with increasing TiO_2 content in the glass. The spectra show a single broad resonance with a "tailed" distribution towards lower frequency (more negative ppm) which lacks any resolution; this is typical of second-order quadrupolar line shapes in glassy materials. The resonance becomes more downfield shifted (more positive ppm) as a result of the second-order quadrupolar effect, which is inversely proportional to the magnet field (B_0) [15].

The tail of the peak can be explained by a distribution of quadrupole interactions [29]. This effect reflects division of local sodium environments within the sample. Using Quadfit, the spectra were deconvoluted to give a central $C_Q \approx 2.7$ MHz (the quadrupolar coupling constant [15,29] and width of $\Delta C_Q = 1.8$ MHz (which represents a measure of the range of C_Q present in the sample) for each of the samples, as expressed in Table 3 [17].

Despite an increasing TiO_2 content the simulated quadrupolar parameters suggest that the distribution of sodium environments are relatively constant in symmetry. This phenomenon has also been observed in the introduction of ZnO to phosphates glasses, where ZnO acts as a network modifier and the role of Na_2O appears unaffected throughout [24].

Fig. 11 shows that on increasing the TiO_2 content the ^{23}Na chemical shift decreases but may not be statistically significantly different.

This can be explained as follows: as the Na_2O content decreases, the glass content becomes more spatially compact, meaning that the average sodium-to-oxygen bond decreases. This decrease

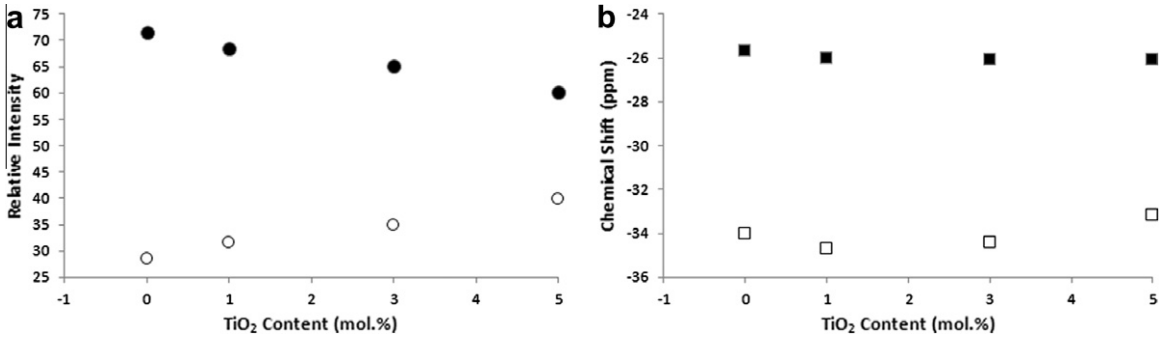

Fig. 9. (a) The abundance of Q^2 units (closed circle) and Q^3 units (open circle) in the phosphate glasses with increasing mol.% TiO_2. (b) The variation in the ^{31}P isotropic chemical shift for Q^2 units (closed squares) and Q^3 units (open squares). (For clarity, the error bars associated with the data have not been plotted.)

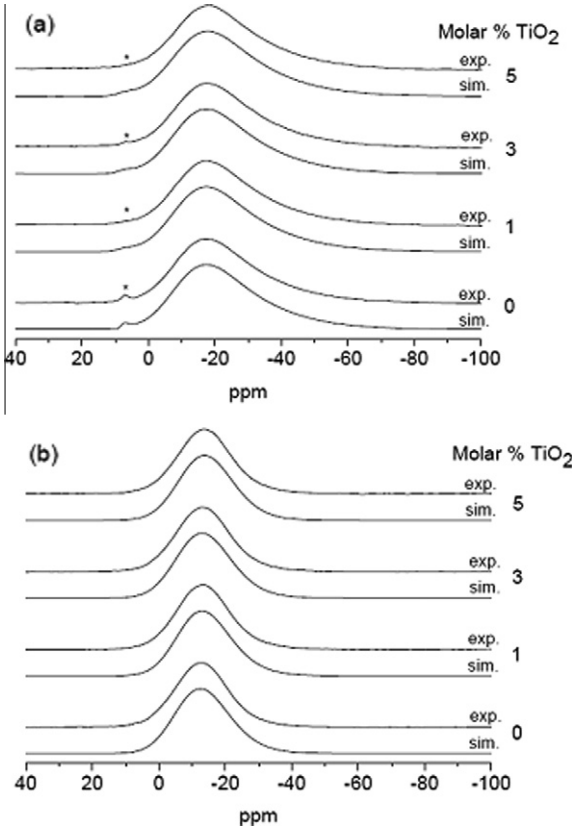

Fig. 10. ^{23}Na MAS-NMR spectra and simulations obtained for the glasses with increasing mol.% TiO_2. The spectra were acquired at (a) 9.4 and (b) 14.1 T.

Table 3
Summary of the ^{23}Na C_Q values, isotropic chemical shifts and P_Q (see Eq. (2)).

TiO_2 content (%)	ΔC_Q (MHz)	C_Q (MHz)	δ_{iso}[a]	δ_{iso}[b]	P_Q (MHz)
0	1.8 ± 0.1	2.7 ± 0.1	−6.3 ± 0.3	−5.4 ± 1	2.8 ± 0.2
1	1.8 ± 0.1	2.7 ± 0.1	−6.6 ± 0.1	−7.2 ± 1	2.6 ± 0.2
3	1.8 ± 0.1	2.7 ± 0.1	−6.8 ± 0.2	−7.1 ± 1	2.7 ± 0.2
5	1.8 ± 0.1	2.6 ± 0.2	−7.5 ± 0.7	−7.4 ± 1	2.6 ± 0.2

[a] Determined using Quadfit.
[b] Determined from the y-intercept of the plot of δ_{cg} vs. B_0^{-2}.

causes a corresponding increase in shielding and hence the isotropic shift is observed at a lower frequency; such an effect has also been observed in other sodium glasses [30].

With multiple magnetic field data, some NMR parameters can be extracted. The quadrupolar parameters (i.e., the quadrupolar coupling constant (C_Q)) can be derived, or more correctly a combination of C_Q and the quadrupolar asymmetry parameter η_Q termed P_Q (the quadrupolar effect parameter), defined as:

$$P_Q = C_Q\sqrt{1+\eta_Q^2/3} \quad (2)$$

may be extracted from the gradient of the plot of the center of gravity (δ_{cg}) of the ^{23}Na resonance against the squared inverse of the magnetic field (B_0^{-2}), as given in Eq. (3) [31]:

$$\delta_{cg} = \delta_{iso} - 25{,}000\frac{C_Q^2\sqrt{1+\eta_Q^2/3}}{(\gamma/2\pi)^2}\cdot\frac{1}{B_0^2} \quad (3)$$

where the δ_{cg} represents the center of gravity (position weighted mean taking into consideration all distributions) and δ_{iso} (the isotropic chemical shift) is the average of the three principal components of the chemical shift tensor as described by the shielding produced due to electron density inside a magnetic field. The P_Q for each of these glasses is similar to the C_Q derived from the Quadfit simulation, thus suggesting that $\eta_Q \sim 0$.

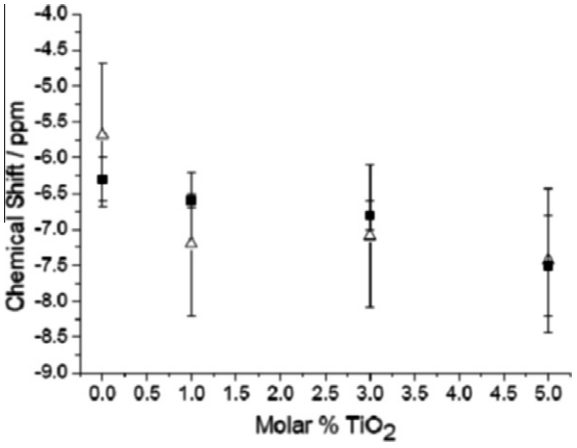

Fig. 11. Dependence of the ^{23}Na isotropic chemical shift (δ_{iso}, ppm) on TiO_2 concentration (mol.%). The isotropic shifts were determined using Quadfit (solid squares) and from the y-intercept of the plot δ_{cg} vs. B_0^{-2} (open triangles).

Solid-state NMR has shown unequivocally the formation of Q^2 and Q^3 phosphate species when the molar percentage of P_2O_5 rises above 50 [11]. This is shown to have had limited effect on the Na_2O environments, except that due to a decrease in the chemical shift, which can be attributed to a decrease of the average Na–O bond length as titanium is added.

4. Conclusion

A key objective of the present study was to better understand the effect of incorporation of TiO_2, substituting for Na_2O, on the structure and physical properties of a series of high-phosphorus-content (55 mol.%) phosphate-based glasses. On adding TiO_2 to the phosphate network of these glasses up to 5 mol.%, thermal stability improved together with an increase in the density. Also there is an increase the glass transition temperature (T_g). Incorporation of TiO_2 was also shown to successfully control the glass degradation rate and hence ion release, which are crucial for the targeted biomaterials applications.

From a structural point of view, XRD data showed the appearance at low levels of crystalline CaP_2O_6 and TiP_2O_7, which are known to be biocompatible [32], upon heat treatment of glasses at their crystallization temperatures. Raman and FTIR studies demonstrated an increase in the formation of P–O–Ti bonds and as a result, a transformation of Q^2 to Q^3 units was observed by addition of TiO_2. This also correlates with enhanced glass stability.

Acknowledgements

This work was supported in part (JCK) by WCU Program through the National Research Foundation of Korea (NRF) funded by the Ministry of Education, Science and Technology (No. R31-10069). The EPSRC are thanked for contributing to the NMR infrastructure as are the University of Warwick including via part funding through Birmingham Science City Advanced Materials Project supported by Advantage West Midlands (AWM) and the European Regional Development Fund (ERDF).

Appendix A. Figures with essential color discrimination

Certain figures in this article, particularly Figures 6, 7 and 9, are difficult to interpret in black and white. The full color images can be found in the on-line version, at doi:10.1016/j.actbio.2011.08.025.

References

[1] Hench LL. Glasses to turn on genes. Glass Sci Technol 2004;77:95.
[2] Knowles JC. Phosphate based glasses for biomedical applications. J Mater Chem 2003;13:2395.
[3] Hench LL, Xynos ID, Polak JM. Bioactive glasses for in situ tissue regeneration. J Biomater Sci Polym Ed 2004;15:543.
[4] Franks K, Salih V, Knowles JC, Olsen I. The effect of MgO on the solubility behavior and cell proliferation in a quaternary soluble phosphate based glass system. J Mater Sci Mater Med 2002;13:549.
[5] Shih PY, Ding JY, Lee SY. P-31 MAS-NMR and FTIR analyses on the structure of CuO-containing sodium poly- and meta-phosphate glasses. Mater Chem Phys 2003;80:391.
[6] Abou Neel EA, O'Dell LA, Smith ME, Knowles JC. Processing, characterisation, and biocompatibility of zinc modified metaphosphate based glasses for biomedical applications. J Mater Sci Mater Med 2008;19:1669.
[7] Bingham PA, Hand RJ, Hannant OM, Forder SD, Kilcoyne SH. Effects of modifier additions on the thermal properties, chemical durability, oxidation state and structure of iron phosphate glasses. J Non-Cryst Solids 2009;355:1526.
[8] Abrahams I, Franks K, Hawkes GE, Philippou G, Knowles JC, Bodart P, et al. Na-23, Al-27 and P-31 NMR and X-ray powder diffraction study of Na/Ca/Al phosphate glasses and ceramics. J Mater Chem 1997;7:1573.
[9] Li YB, Weng WJ, Santos JD, Lopes AM. Structural studies of Na_2O-TiO_2-CaO-P_2O_5 system glasses investigated by FTIR and FT-Raman. Phys Chem Glasses Eur J Glass Sci Technol B 2008;49:41.
[10] Abou Neel EA, Knowles JC. Physical and biocompatibility studies of novel titanium dioxide doped phosphate-based glasses for bone tissue engineering applications. J Mater Sci Mater Med 2008;19:377.
[11] Kiani A, Cahill LS, Abou Neel EA, Hanna JV, Smith ME, Knowles JC. Physical properties and MAS-NMR studies of titanium phosphate-based glasses. Mater Chem Phys 2010;120:68.
[12] Nan Y, Lee PF, James J. Crystallization behavior of CaO-P_2O_5 glass with TiO_2, SiO_2, and Al_2O_3 additions. J Am Ceram Soc 1992;75:1641.
[13] Navarro M, Ginebra M, Clement J, Martinez S, Avila G, Planell JA. Physicochemical degradation of titania-stabilized soluble phosphate glasses for medical applications. J Am Ceram Soc 2003;86:1345.
[14] International Center for Diffraction Data Powder diffraction database, vols. 1–42; 1992.
[15] MacKenzie KJD, Smith ME. Multinuclear solid state NMR of inorganic materials. Oxford: Pergamon; 2002.
[16] Massiot D, Fayon F, Capron M, King I, Le Calve S, Alonso B, et al. Modelling one- and two-dimensional solid-state NMR spectra. J Magn Reson Chem 2002;40:70.
[17] Kemp TF, Smith ME. QuadFit-A new cross-platform computer program for simulation of NMR line shapes from solids with distributions of interaction parameters. Solid State Nucl Magn Reson 2009;35:243.
[18] Dias AG, Costa MA, Lopes MA, Santos JD, Fernandes MH. Biological activity of two glass ceramics in the meta- and pyrophosphate region: a comparative study. In: Barbosa MA, Monteiro FJ, Correia R, Leon B, editors. Bioceramics 16. Zurich-Uetikon: Trans Tech Publications Ltd; 2004. p. 825–8.
[19] Brow RK. Review: the structure of simple phosphate glasses. J Non-Cryst Solids 2000;263:1.
[20] Valappil SP, Ready D, Abou Neel EA, Pickup DM, Chrzanowski W, O'Dell LA, et al. Antimicrobial gallium-doped phosphate-based glasses. Adv Funct Mater 2008;18:732.
[21] Carta D, Pickup DM, Knowles JC, Ahmed I, Smith ME, Newport RJ. A structural study of sol-gel and melt-quenched phosphate-based glasses. J Non-Cryst Solids 2007;353:1759.
[22] Shih PY. Properties and FTIR spectra of lead phosphate glasses for nuclear waste immobilization. Mater Chem Phys 2003;80:299.
[23] Karabulut M, Metwalli E, Day DE, Brow RK. Mossbauer and IR investigations of iron ultraphosphate glasses. J Non-Cryst Solids 2003;328:199.
[24] Abou Neel EA, Chrzanowski W, Valappil SP, O'Dell LA, Pickup DM, Smith ME, et al. Doping of a high calcium oxide metaphosphate glass with titanium dioxide. J Non-Cryst Solids 2009;355:991.
[25] Brow RK, Kirkpatrick RJ, Turner GL. The Short Range Structure of Sodium-phosphate Glasses.1. MAS NMR-Studies. J Non-Cryst Solids 1990;116:39.
[26] Franks K, Abrahams I, Knowles JC. Development of soluble glasses for biomedical use Part I: In vitro solubility measurement. J Mater Sci Mater Med 2000;11:609.
[27] Salih V, Franks K, James M, Hastings GW, Knowles JC, Olsen I. Development of soluble glasses for biomedical use Part II: The biological response of human osteoblast cell lines to phosphate-based soluble glasses. J Mater Sci Mater Med 2000;11:615.
[28] Stebbins JF, Farnan I, Xue XY. The Structure and Dynamics of Alkali Silicate Liquids. A View From NMR-Spectroscopy. Chem Geol 1992;96:371.
[29] Smith ME, Van Eck ERH. Recent advances in experimental solid state NMR methodology for half-integer spin quadrupolar nuclei. Prog Nucl Magn Reson Spectrosc 1999;34:159.
[30] Zuchner L, Chan JCC, Muller-Warmuth W, Eckert H. Short-range order and site connectivities in sodium aluminoborate glasses: I. Quantification of local environments by high-resolution B-11, Na-23, and Al-27 solid-state NMR. J Phys Chem B 1998;102:4495.
[31] Samoson A. Two-dimensional isotropic NMR of quadrupole nuclei in solids. J Magn Reson Ser A 1996;121:209.
[32] Dias AG, Skakle JMS, Gibson IR, Lopes MA, Santos JD. In situ thermal and structural characterization of bioactive calcium phosphate glass ceramics containing TiO_2 and MgO oxides: High temperature XRD studies. J Non-Cryst Solids 2005;351:810.